A Study of Concrete Specimen Change Under Fracture

T. Zhang[1], W.R. Franklin[1], E. Landis[2], E. Nagy[2] and G. Nagy[1]

Rensselaer Polytechnic Institute, Troy, NY, USA [1]
University of Maine, Orono, ME, USA [2]
E-mail: zhangt2@rpi.edu

Abstract

Volumetric images of small mortar cylinders under load are acquired by X-ray microtomography. The images are binarized at different threshold values, and the connected components are extracted at each threshold with a 3D space- and time-efficient program. Statistics of volume and surface area of separated concrete segments and cracks are collected and analyzed. Under increasing load, the concrete specimen can undergo size distortion. The largest segments and cracks account for 99% of the change. Some segments and cracks merge.

1. Introduction

Concrete is widely used. Understanding why and how concrete fractures has been of great interest to physicists, civil engineers and material scientists. Even though the application of fracture mechanics to concrete has progressed [1], much remains unknown. While continuum approaches based on plasticity and linear elastic fracture mechanics have led to considerable success in predicting failure in fine-grained materials such as metals, non-linear effects have resisted analysis in heterogeneous and quasi-brittle materials such as concrete. The study of microstructure coupled with traditional stress-strain measurements offers the most promising approach.

In [7], we analyzed thin, warped, interconnected cracks in sequences of density images of samples of mortar. Now we report the application of image processing techniques to locate and measure the changes in the separated segments due to cracks, and the overall change properties of concrete specimen under fracture.

The resulting measurements will ultimately be used in multiscale modeling of the microstructure for improved understanding of the macroscopic mechanical properties of concrete fracture.

2. Data Collection

The data was collected and preprocessed by the University of Maine team [6] at Beamline X2B in Brookhaven National Laboratory using X-ray microtomography [10, 4, 3]. XMT is used to measure the internal X-ray absorption of a 3D object. It is similar to a medical CAT scan, except for the much higher beam intensity and detector resolution. The high energy beam is generated using synchrotron radiation rather than the X-ray tubes used in the conventional CAT scan.

The concrete specimens are small motar cylinders about 4 millimeters in diameter and 4 millimeters in height. The specimen is a mixture of Type I portland cement, sand and water. It consists of solids (sand, cement and aggregate) and voids (cracks and air holes).

The concrete specimen is held on a rotational stage in a specially designed apparatus (Figure 1(a)). An uniaxial compressive load is then applied to the specimen by piezoelectric crystals. The stress is continuously monitored by a conventional load cell.

The X-ray beam is monochromated by a silicon crystal to select the energy of 32 keV. For optimum contrast, this energy is chosen such that 90% is absorbed by the specimen. As in a CAT scan, the rotational stage is designed to allow load application with minimum X-ray absorption.

The X2B's detector has a single-crystal phosphor with high spatial resolution. It converts the X-ray to visible light (Figure 1(b)). The light is detected by a 1024×1024 pixel CCD camera to generate an absorption map. The specimens were exposed to the beam at 720 different angles over 180° and maps of absorptivity were generated at each angle.

After applying Exxon Direct Fourier Reconstruction to the absorption maps, the result is quantized to generate the final data set, which is a grayscale 3D volume with one byte per voxel.

The same process is applied to the concrete specimen with 5 or 6 load-and-release cycles, with progressively greater loads. The last volume is supposed to capture the state of the specimen after the peak of the stress-strain

curve, before it crumbles with any further load. A new data set is generated at each stage.

Two volumetric data sets from successive loads, $T1$ and $T2$, were analyzed. The volume of each data set is $800 \times 800 \times 765$ at $(6\mu m)^3$/voxel. Figure 1 (c,d) shows two slice images from these two volumes at corresponding horizontal cross sections, where the specimen was separated into segments due to the cracks.

The grayscale of each voxel corresponds to the X-ray absorption at that particular point in the specimen. The brighter the voxel is, the higher its density. At this resolution, some concrete microstructures can be distinguished: the dark low density regions are voids (cracks and air holes); the bright high density regions are sand; the gray regions are cement and aggregates.

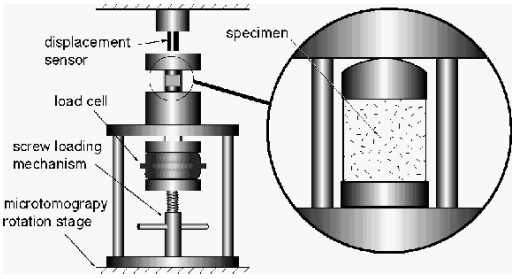

(a)

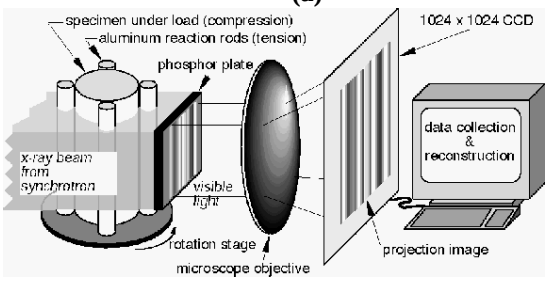

(b)

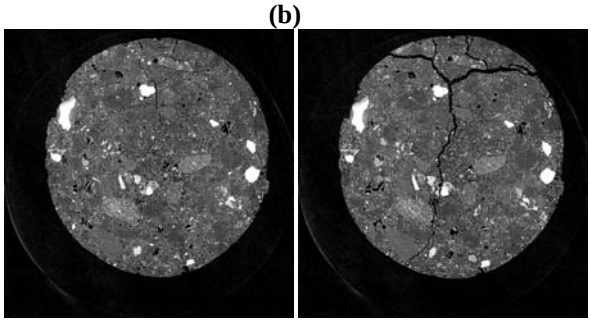

(c) **(d)**

Figure 1. (a) The load cell for holding the concrete specimens under calibrated loads; (b) The system for X-ray microtomography; (c,d) Two grayscale images of $T1, T2$ at corresponding horizontal cross sections.

3. Data Analysis

Because of the large volume of data ($\sim 5 \times 10^8$ voxels), binarization followed by connected component (CC) analysis [8, 9, 2] is the most practical means of investigating the foreground material (mortar, sand, aggregate) and background void (cracks and air holes) constituents of the specimen.

We used a space- and time-efficient CC algorithm with Find-Union on 1-D runs and path compression [5]. It finds, in each CC, the constituent voxels, number of runs, volume and surface area (number of free faces). In order to preserve topological integrity, we used 6-connectivity (face) for foreground (segment), and 26-connectivity (vertex) for background (crack).

The complex photometric, geometric and topological properties of each specimen are deduced by observing the cardinality, volume, surface area and surface area to volume ratio of foreground and background CCs obtained over the entire range of binarization thresholds. The volume change of each segment is an indication of distortion under stress. Since the external force is expected to equal the work required to stretch the internal surfaces, the surface area increase in segments is also an important parameter. Furthermore, the ratio $A^{\frac{3}{2}}/V$, a *shape invariant*, is a useful measure of compactness and rotundity.

The remaining sections present the observations in detail.

3.1. Density

As can be seen in Figure 2(a), the voxel densities in $T1$ and $T2$ both have a slightly flattened Gaussian distribution with $\mu = 96.7$, and $\sigma = 43.5$ for $T1$, and $\mu = 95.5$, and $\sigma = 44$ for $T2$, respectively.

As reported previously, the observed density is partly the result of low-pass filtering by the relatively large point spread function of 3-D digitizing system [7].

3.2. Connected Component Distributions

At any threshold, there are a large number of segment and crack CCs. As seen from Figure 2(b), the number of segment CCs peaks at threshold $\theta = 123$, while the number of crack CCs peaks at $\theta = 46$. There are about the same number of segment and crack CCs near $\theta = 96$.

As θ increases from 2 to 46, small cracks emerge. The cracks then merge by narrow connections that were smoothed initially by the point-spread function, and "islands" of material segment become visible. Above $\theta = 123$, we see the consolidation of various types of material segment (mortar, sand, aggregate) that have different densities.

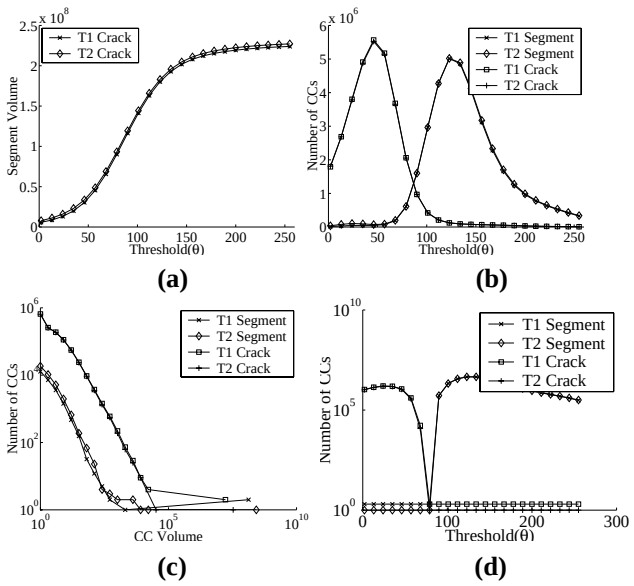

Figure 2. Statistics of $T1, T2$ against binarization threshold: (a) Background volume; (b) Number of CCs; (c) Distribution of number CCs at $\theta = 46$; (d) Minimum number of CCs covering $\geq$99% of total foreground and background volume.

The CCs at any specific threshold appear to have an exponential distribution: most of the CCs have very small volume, and the number of CCs drops drastically as the CC volume increases. This fact is more obvious from the logarithmic plot of the numbers of segment and crack CCs versus CC volume at $\theta = 46$ in Figure 2(c). This property is persistent at other thresholds.

3.3. Dominant Components

Despite the large number of CCs, the minimum number of CCs covering at least 99% of total foreground and background volume can be very small (Figure 2(d)).

If we call them *dominant*, then at $\theta \leq 79$, there are only two dominant segments in $T1$ and one dominant segment in $T2$; at $\theta \geq 79$, there are only two dominant cracks in $T1$ and one dominant crack in $T2$.

In Figure 3, the results are shown with one slice of $T2$ binarized at $\theta = 46, 79, 123$, respectively. At $\theta = 46$, the cracks are disconnected because of binarization; at $\theta = 123$, we see the consolidation of aggregates and sand, but the cracks have disappeared; at $\theta = 79$, both segments and cracks are identifiable.

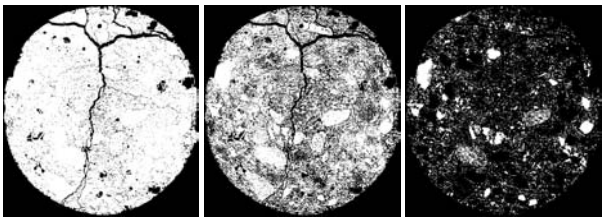

Figure 3. Sample slice image of $T2$ binarized at different thresholds: (a) $\theta = 46$; (b) $\theta = 79$; (c) $\theta = 123$.

Table 1. Volume of the largest CCs at $\theta = 79$.

Volume	$T1$	$T2$
Total Foreground	$135,955,338$	$136,024,620$
Largest segment CC	$72,356,206$ (53.2%)	$134,891,432$ (99.2%)
2nd Largest segment CC	$62,503,423$ (46.0%)	
Total Background	$90,114,788$	$93,234,122$
Largest crack CC	$48,391,026$ (53.7%)	$92,890,622$ (99.6%)
2nd Largest crack CC	$41,382,361$ (45.9%)	

3.4. Specimen Volume Growth

Two largest segment CCs in $T1$ and one largest segment CC in $T2$ cover $> 99\%$ of the foreground volume (Table 1), while the remaining $605,998$ segment CCs in $T1$ and $613,490$ segment CCs in $T2$ cover only 1% of $T1$ and $T2$ foreground, respectively.

Similarly, two largest crack CCs in $T1$ and one largest crack CC in $T2$ cover $> 99.5\%$ of the background volume (Table 1), while the remaining $2,061,841$ crack CCs in $T1$ and $2,051,038$ crack CCs in $T2$ cover only 0.5% of $T1$ and $T2$ background, respectively.

Since the specimen volume is the sum of segment and crack volume, the specimen volume has increased by $3,188,616$ or 1.4%, of which $31,803$ or 1% is caused by increase in the largest segment CCs, and $3,117,235$ or 97.8% is caused by the growth of the largest crack CCs. The growth of the largest CCs accounts for almost 99% of the enlargement of the entire specimen. Therefore, focusing on the largest segments and cracks will suffice to analyze the change in the specimen under load. In particular, the specimen's enlargement can be attributed mostly to the widening of the largest cracks.

Under increasing load, the largest two segments and cracks in $T1$ have merged in $T2$.

Table 2. Volume, surface area, and surface area to volume ratio of the largest CC's at threshold 79.

Segment CC		Largest	2nd Largest
$T1$	Volume V	$72,356,206$	$62,503,423$
	Surface Area A	$114,087,980$	$102,814,934$
	Ratio $A^{\frac{3}{2}}/V$	16842	16679
$T2$	Volume V	$134,891,432$	
	Surface Area A	$217,486,828$	
	Ratio $A^{\frac{3}{2}}/V$	23777	
Crack CC		Largest	2nd Largest
$T1$	Volume V	$48,391,026$	$41,382,361$
	Surface Area A	$115,909,634$	$103,776,020$
	Ratio $A^{\frac{3}{2}}/V$	25788	25546
$T2$	Volume V	$92,890,622$	
	Surface Area A	$220,697,504$	
	Ratio $A^{\frac{3}{2}}/V$	35296	

3.5. Segment and Crack Compactness

In compact objects, most of the voxels would be either interior voxels with 0 free face, or surface voxels with 1 free face. For example, for a sphere of radius r, volume V, surface area A, the ratio $A^{\frac{3}{2}}/V$ will be $6\sqrt{\pi} \sim 10.6$. For a cube, the ratio will be $6^{1.5} = 14.7$. This ratio can be used to measure compactness of connected components. The smaller the ratio is, the more compact is the component.

We calculated the above ratio for the largest CCs. The results are listed in Table 2. It can be seen that the segments are more compact than the cracks. At the same time, the enormous ratios indicate that the CCs are not only tortuous, but highly porous as well.

4. Conclusions and Future Work

With a fast CC program and thresholding, we quantitively analyzed the 3D concrete data and found that:

1. The concrete specimen under fracture consists of very few large segments and cracks. Other than these larger ones, there is also a huge number of much smaller segments and cracks. Despite their large quantity, these small segments and cracks occupy less than 1% of the whole volume.

2. Under increasing load, the concrete segment volume barely changes, although segments undergo movement due to the widening of cracks. The increase in specimen volume is caused mainly by the growth of cracks. It is also observed that segments and cracks merge when the load increases.

3. Although the segments are more compact than cracks, they both are extremely tortuous and porous with enormous $A^{\frac{3}{2}}/V$ ratio, indicating both having honeycomb-like structures.

We have much work ahead of us. Other than thresholding, we would like to explore segmentation techniques that can provide a better discrimination between segments and cracks. We don't yet have any effective measures of segment and crack shape and topology. Furthermore, current 3D image registration techniques will have to be extended to the compound problem of bringing into correspondence objects exhibiting both global distortion (motion of the sample) and local changes due to segment distortion and crack growth.

Another important issue is the pore structure connectivity that governs water penetration from the concrete surface. If we are able to discriminate segments and cracks inside the specimen, we can determine which cracks open to the surface. By tracing these cracks, we can compute what fraction of the volume is at a given distance from the surface. Our long-term goal is the parameterization of change in concrete under fracture for multiscale modeling and analysis.

References

[1] Z. P. Bazant. *Fracture Mechanics of Concrete Structures*. Elsevier Applied Science, 1992.

[2] G. Borgefors, I. Nystrom, and G. S. de Baja. Connected components in 3d neighborhoods. In *Procs. 10th Scandinavian Conf. on Image Analysis(SCIA'97)*, pages 557–570, Helsinki, 1997.

[3] H. Deckman, J. Dunsmuir, K. D'Amico, S. Ferguson, and B. Flannery. Development of quantitative x-ray microtomography. In *Materials Research Society Symposium Proceedings*, volume 217, pages 97–110, 1991.

[4] B. Flannery, H. Deckman, W. Roberge, and K. D'Amico. Three-dimensional x-ray microtomography. *Science*, 237:1439–1444, 1987.

[5] W. R. Franklin. Connect - find 3d connected components. http://www.ecse.rpi.edu/homepages/wrf/research/connect/.

[6] E. N. Landis, E. N. Nagy, D. T. Keane, and G. Nagy. Technique to measure 3d work-of-fracture of concrete in compression. *Journal of Engineering Mechanics*, 125(6):599–605, June 1999.

[7] G. Nagy, T. Zhang, W. R. Franklin, E. Landis, and D. Keane. Volume and surface area distributions of cracks in concrete. In *4th International Workshop on Visual Form*, Capri,Italy, May 2001.

[8] C. Ronse and P. Devijver. *Connected components in binary images: the detection problem*. Research Studies Press, Letchworth, England, 1984.

[9] H. Samet. *Applications of Spatial Data Structures*. Addison-Wesley, 1989.

[10] F. Slate and S. Olsefski. X-ray study of internal structure and microcracking of concrete. *J.Am. Concrete Inst.*, 60(5):575–588, 1963.